Materials Research Express

PAPER

Mg-X (X = Ni, Pd, Ti, Nb) interface and atomic mixture effect: a first-principles study

RECEIVED
22 August 2018

REVISED
25 September 2018

ACCEPTED FOR PUBLICATION
1 October 2018

PUBLISHED
12 October 2018

Yanan Wu[1], Xiaotian Li[1], Zhongjia Chen[1], Jusong Yu[1], Shaobin Qiu[1], Xiao-Bao Yang[1,2] and Yu-Jun Zhao[1,2]

[1] Department of Physics, South China University of Technology, Guangzhou 510640, People's Republic of China
[2] Key Laboratory of Advanced Energy Storage Materials of Guangdong Province, South China University of Technology, Guangzhou 510640, People's Republic of China

E-mail: zhaoyj@scut.edu.cn

Keywords: first-principles calculation, interface stability, atomic mixture effect, diffusion barrier

Abstract

The structure stabilities and electronic properties of Mg-X (X = Ni, Pd, Ti, Nb) interfaces are studied by first-principles calculations, including the atomic mixture effect. In particular, the Mg-X interface structures are systemically investigated by minimizing the lattice mismatch, including the lattice constants, cell area, and included angle of the lattice (cell shape). It is found that the optimal interface matches are 4:7, 3:4, 7:8, 9:4 in surface cell atom numbers (limited up to 10 in consideration of computational cost) for Mg-Ni, Mg-Pd, Mg-Ti, Mg-Nb, and the corresponding interface energies are -0.01, -0.9, 0.4, 0.9 J m^{-2}, respectively. We find that atomic mixing at the interface affects the strain, and even stablize the interfaces in the large-mismatch cases. Furthermore, exemplified with the Mg-Pd interface, we find the atoms at the interface can be exchanged under practical condition with assitance of vacancies at the interface.

1. Introduction

Mg alloys have been persistently attractive for the widespread application in industries, including the aerospace, appliance, medical, automotive and new energy storage industries [1, 2], due to its low specific gravity, high strength and earth abundance [3, 4]. Researches show that the interface of Mg and transition metals plays an important role in various applications, including the improvement of hydrogen energy storage performance [5]. It was reported that Mg-Ti interface strongly interacts with H to strengthen the hydrogen adsorption ability with respect to Mg [5, 6], and the interfacial fugacity would enhance hydrogenation reaction rate in Mg-Ni layers [7]. Excellent thermodynamic properties have been demonstrated for the magnesium films covered with Pd [8]. It is clear that Mg-X interfaces are significantly important for characteristics of thermodynamic properties and hydrogen absorption performance.

The internal stress is ubiquitous resulting from lattice mismatch in the heteroepitaxial structures [9]. It is critical to explore a proper approach to construct Mg-X interface models and analyze the structure and electronic properties, considering the Mg interface with miscible or immiscible metals. Usually, if the lattices of two phases have the same shape and a small mismatch, the lattice of the softer compound is often adjusted to near the harder one to build a coherent interface [10, 11]. In general, however, the shapes of lattice are also different from each other, involving the revolution of phase lattice to achieve a reasonable match in the interface [12]. Obviously, a rational interface model should be optimized with a minimum interface energy [13], followed by most interface studies of Mg-X, including Mg-Ti [6], etc.

Practically, the plastic working of combination of Mg alloying causes various defects at the interface, such as vacancies, atomic mixture, whose formation are always involved with diffusion. Interestingly, it has been demonstrated that vacancies in Mg significantly often enhance the diffusion of other impurity atoms with respect to the perfect crystal lattice [14]. The impact of impurity diffusion in magnesium has also attracted much attention to the macroscopic Mg alloys properties, such as castability and strengthening [15–17]. Nowadays, there are a number of studies on the diffusion of impurities in magnesium bulk available, including experiments

and theoretical calculations of vacancy formation energy in Mg, solute-vacancy binding energy and diffusion energy barrier of some dilutes [1, 18–20]. A methodology of computing the diffusion coefficients for dilutes (Ca, Al, Sn) in Mg with some vacancies is presented in literature [21]. Researchers mainly paid attention to dilutes diffusion in magnesium bulk, while the studies of diffusion properties at the interface of Mg and other metals were often neglected, partially due to the complexity of interface structures [22]. Nevertheless, the atomic mixture effect, and the corresponding possible diffusion path in the Mg-X interfaces has not been seriously addressed, although it clearly affects the interface structure and properties.

In this paper, we have adopted first-principles approach to study the interface of Mg-X, including the mixture effect, for miscible (X = Ni and Pd) and immiscible metal elements (X = Ti and Nb). We have constructed the Mg-X interface structures systemically by minimizing the lattice mismatch. As expected, we find that the interfaces of Mg with miscible phases are more stable than those with immiscible metals. In the case of large lattice mismatches, atomic mixing in the interface remarkably reduces the interface energy for both miscible and immiscible metals with Mg. Additionally, we find that the atoms in interface are exchanged with assistance of vacancies under practical conditions.

2. Computational methods

Density functional theory (DFT) as implemented in Vienna *Ab initio* Simulation Package [23, 24] (VASP) is employed to perform the calculations. Projector augmented wave (PAW) method [25] with the Perdew, Burke, and Ernzerhof (PBE) [26] generalized gradient approximation functional is adopted. The plane-wave cutoff energy is set to be 300 eV, which meets the conditions of interface energy convergence for the four models. For example, the interface energy difference is within 0.015 J m^{-2} when the cutoff energy increases from 300 eV to 600 eV for Mg-Ti interface model. 5 × 5 × 1 Monkhorst-Pack k-point grid [27] for Mg-Pd and Mg-Ni interface models, and 3 × 3 × 1 for Mg-Nb and Mg-Ti interface models are used. The convergence criterion for the structural relaxation is set to 0.01 eV $Å^{-1}$.

The climbing image nudged elastic band (CI-NEB) method is used to calculate the minimum energy path for the atom transition in the interface. At least five images are simultaneously optimized to obtain the transition energy barrier and the minimum energy path. The force convergence criterion for every atom of each image is set as 0.01 eV $Å^{-1}$ during the optimization.

3. Results and discussion

3.1. Stability of Mg (0001)-X Interface

It is known that (0001) is the energetically favored surface, which is close-packed, for magnesium. To construct the interface of Mg (0001) with metals X (X = Ni, Pd, Ti and Nb), it requires the two phases share the same shape and similar lattice constants. Fortunately, Ni(111), Pd(111), Ti(0001) and Nb(111), the energetically favored close-packed surfaces have the same shape with Mg(0001). Even so, it is still complicated to obtain the optimal structure match of Mg-X interfaces as the magnitude of their surface lattice constants of a and b, as well as their included angle can be adjusted. For simplicity, we may put restrictions of $a = b$ and their included angle at 60° at the first step.

Here the 'stress balancing' approach is adopted to set up the mutual lattice constant to construct the periodical interface model [28]. It implies that the total energy of the two independent slabs of Mg and X is minimized with respect to the mutual lattice constant. Following the structural optimization of the slabs, we have the optimal mutual lattice parameters of 6.50 Å, 5.57 Å, 8.66 Å, 9.46 Å for Mg-Ni, Mg-Pd, Mg-Ti and Mg-Nb interface models, respectively. The corresponding lattice constants of c are fully optimized accordingly. This approach should be more realistic than the models adopted in earlier literature, where the average of lattice constants of two phases was chosen for the mutual lattice constant of the interfacel [5, 6].

All the possible surface unit cells are with lattice constants of nearest neighbor (NB), a_0, next NB ($\sqrt{3}\,a_0$), 3rd NB ($2\,a_0$) distance, etc, with all the two dimensional unit cells of less than 10 atoms shown in figure 1. Their corresponding optimal lattice match can also be obtained, as listed in table 1. Among these interface models, the 4-atom Pd(111) cell has less than 1% mismatch with the 3-atom Mg(0001) cell, while Ti(0001) has the greatest mismatch of 4.1% with its 9-atom cell matching 7-atom Mg(0001) cell. Ni(111) has the best mismatch of 2.8% with its 7-atom cell matching 4-atom Mg(0001) cell and the 4-atom Nb(111) cell have the best mismatch of 2.4% with the 9-atom Mg(0001) cell.

Furthermore, we removed the restriction of $a = b$, and systematically searched the optimal match of Mg-X interfaces by a code according to the mismatches of cell area, magnitude of lattice vectors, and their included angles for surface cells with atoms less than 10, in consideration of computational cost for DFT simulation of the interfaces. We do find some matches with smaller area mismatches, but no better lattice match found with

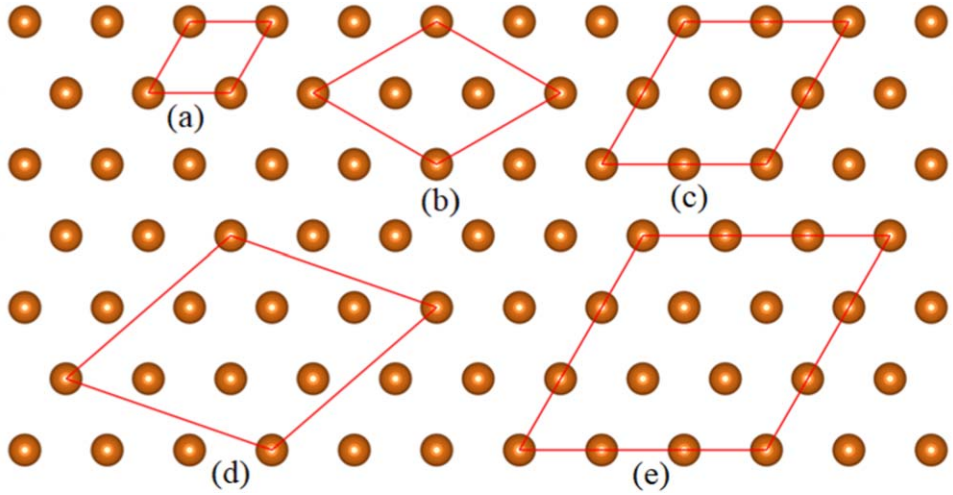

Figure 1. The surface cell selection of Mg or X system on their close-packed surface. Plots (a) to (e) are cells with 1, $\sqrt{3}$, 2, $\sqrt{7}$, 3 times of the primitive lattice constant a_0, respectively.

Table 1. The expansions of the lattice constant relative to the unit cell lattice constant for each phase and the corresponding lattice constants are listed (c.f. figure 1). Considering the computing resource, the expansion multiples of lattice constant are limited with surface cell atoms under 10. The best match ratio and corresponding mismatch (wrt Mg) for each Mg-X interface systems are listed as well.

Multiple of a_0 Phase	1	$\sqrt{3}$	2	$\sqrt{7}$	3	Optimal match (Mg:X)	Lattice mismatch (wrt Mg)
Mg(0001)	3.19	5.53	6.38	8.44	9.57	—	—
Ni(111)	2.48	4.30	4.96	6.56	7.44	$2:\sqrt{7}$	+2.8%
Pd(111)	2.79	4.83	5.58	7.38	8.37	$\sqrt{3}:2$	+0.9%
Ti(0001)	2.93	5.07	5.86	7.75	8.79	$\sqrt{7}:3$	+4.1%
Nb(111)	4.67	8.08	9.34	12.36	14.01	3:2	−2.4%

respect to those listed in table 1 or the number of atoms in the model is much larger than those in table 1. For instance, an 8-atom cell of Ti(0001) (with $a = 2\,a_0$, $b = \sqrt{13}\,b_0$ included angle $= 76°$) has 3.6% area mismatch to a 7-atom cell of Mg(0001) (with $a = \sqrt{3}\,a_0$, $b = \frac{\sqrt{53}}{2}b_0$, included angle $= 76°$), smaller than the 8.4% area match of the optimal match listed in table 1. The corresponding lattice mismatches for a and b from the code searched reach +6%, and −8%, respectively, with the magnitude much greater than the optimal 4% mismatch from table 1. Interestingly, the interface energy of 3.6% mismatch is lower than the optimal choice in table 1, and we will discuss it later together with the mixing effect in section 3.3. Besides, a 7-atom cell of Mg and a 9-atom Pd have 1.8% area mismatch, slightly less than the 2% area mismatch of the optimal choice listed in table 1. We do not consider this Mg-Pd match due to its heavy computational cost and little gain on optimal match. Here, the optimal structural matches with $a = b$ listed in table 1 are adopted for the Mg-X interface study firstly for an easier comparison between the various systems.

Consequently, the interfaces are modeled with the Mg-X slabs of 6 layers each stacking periodically along c direction without vacuum. The convergence of the number of layers is tested with the interface energy. For example, it changes within 0.03 J m^{-2} for Mg-Ti interface when 8 layers of both Mg and Ti are used in the model.

Clearly, the structural stability of the interface is also affected by the different stacking of two phases, i.e., the relative position of two phases of the interface [29]. In order to get the most stable stacking of the atoms at interface, relative displacement along a and b directions of X phase is carried out with respect to the Mg surface.

Following the above settings of the Mg-X interface model, we have calculated the work of adhesion and interface energies to assess their stability. The work of adhesion W_{ad} is a quantity to estimate the interaction between the two phases as defined by the following equation [30–32]:

$$W_{ad} = (\mathrm{E}^{\mathrm{tot}}_{\mathrm{Mg/X}} - \mathrm{E}^{\mathrm{slab}}_{\mathrm{Mg}} - \mathrm{E}^{\mathrm{slab}}_{\mathrm{X}})/2S$$

where $\mathrm{E}^{\mathrm{slab}}_{\mathrm{Mg}}$ and $\mathrm{E}^{\mathrm{slab}}_{\mathrm{X}}$ is the total energy of isolate Mg and X surface systems with corresponding strain while $\mathrm{E}^{\mathrm{tot}}_{\mathrm{Mg/X}}$ is the total energy of Mg-X interface. It is necessary to be divided by two times of the interface area S as two interfaces are included in the unit cell of the interface model.

The calculated work of adhesion of different stacking are shown in figure 2. Mg phase is fixed while shifting X phase along a and b directions to to calculate their work of adhesion with different displacement. The

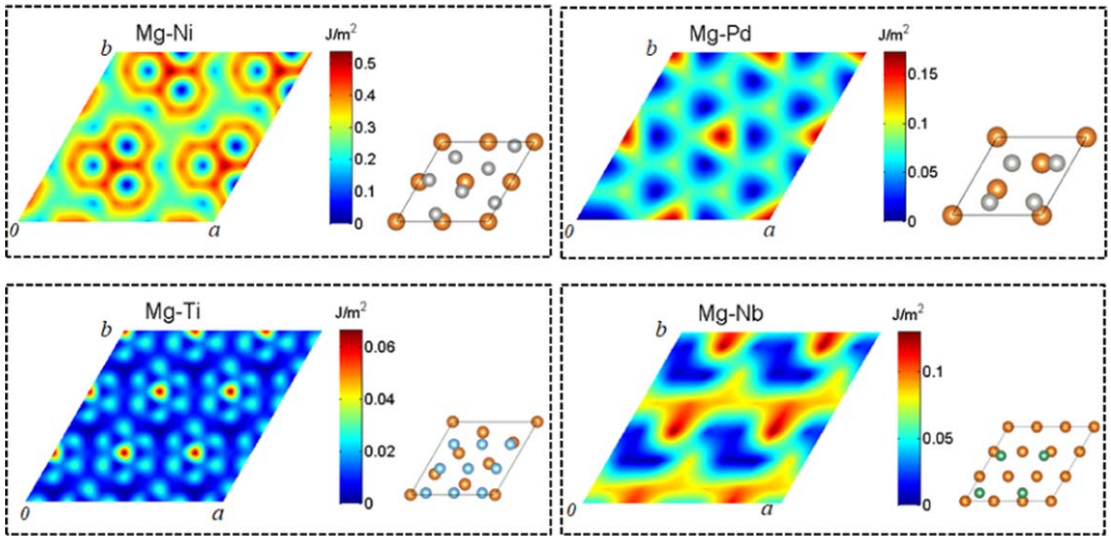

Figure 2. Contour maps showing the difference of work of adhesion (W_{ad}) with respect to the relative position of two phases reflecting the stacking effect on Mg (0001)-X interface. The origin of the energy contour plot is corresponding to the direct stacking of surface cells shown in figure 1, and the inserted interface structures at the right corners are corresponding to the energetically favored stacking. Here Mg atoms are illustrated by the golden balls.

structures corresponding to the origin points are the cells stacking with atoms at the top aligning to each other (c. f. figure 1). The structures with the lowest interface energy (the structure corresponding to the deep blue region) are inserted in figure 1. It is observed that different stacking does not change the work of adhesion significantly for these interfaces. The largest difference of adhesion is just greater than 0.15 J m^{-2} only for Mg-Pd and Mg-Nb systems, while 0.6 J m^{-2} for Mg-Ni system. Specifically, the largest difference of adhesion energy for Mg-Ti interface model is less than 0.07 J m^{-2}, which reflects that the binding energy of Mg and Ti atoms is the smallest among the four systems.

The calculated work of adhesion of the four interface models are shown in figure 3(a) based on the above models. To reflect the stability of the interface, the interface energy is also calculated following the definition of earlier literature [29]:

$$E_{int} = (E^{tot}_{Mg/X} - E^{bulk}_{Mg} - E^{bulk}_{X})/2S$$

E_{int} represents the interface energy of Mg-Ni, Mg-Pd, Mg-Ti, or Mg-Nb model. E^{bulk}_{Mg} and E^{bulk}_{X} are the energies of Mg and X bulk structures with the same stretch as in interface models correspondingly. As shown in figure 3(a), the W_{ad} of all interface systems is negative. It implies that the two phases attract to each other even for the immiscible Mg-Ti and Mg-Nb, mainly contributing to the surface energies. It shows that the four interfaces will be stabilized experimentally as long as the corresponding surfaces can be cleaved. According to figure 3(b), it is clear that the interface energies of Mg-Ni and Mg-Pd slab structure models are all negative, i.e., their slab models are energetically favored with respect to their individual bulk structures with the corresponding stretch. It can be explained that Pd and Ni prefer to be combined into strong bonds with Mg atoms in the interface to stabilize the structure, as Pd-Mg more energetically favored. It is worth noting that the interface energy of Mg-Ni system is almost negligible, 0.01 J m^{-2}. In contrast, the interface energies of Mg-Ti and Mg-Nb slab structures are higher and are unstable with respect to their individual elemental crystals. This is in consistent with the fact that Pd and Ni are miscible with Mg while Ti and Nb are not.

The structural properties such as the spacing between layers for the Mg-X interface models and Mg, X isolated surface models under corresponding strains are given in table 2. In general, it is seen that when the interfaces form for Mg-Ni and Mg-Pd models, the spacing between Mg-Mg and X-X layers increase due to the miscibility effect and the stretching effect on layers farther away from interface. For example, the spacing of Mg 1/2, Mg 2/3, Mg 3/4, Ni 2/3, Ni 3/4 of Mg/Ni interface model all increase except Ni 1/2, compared with Mg and Ni surface with the same strain. This is due to the attracting effect of the interface and corresponding stretch effect of the layer of Mg and Ni phases. Similarly, for Mg/Pd interface model, the spacing between Mg 2/3, Mg 3/4, Pd 1/2, Pd 2/3 and Pd 3/4 are all widen except Mg 1/2 keeping the same spacing with the pure surface model. In contrast, the spacing between layers near interface would be compressed for Mg-Ti and Mg-Nb interfaces, due to the immiscibility effect in interface and corresponding squeezing effect on layers farther away from interface. Although the structure change for Mg-Ti interface model is not obvious, among the six layer

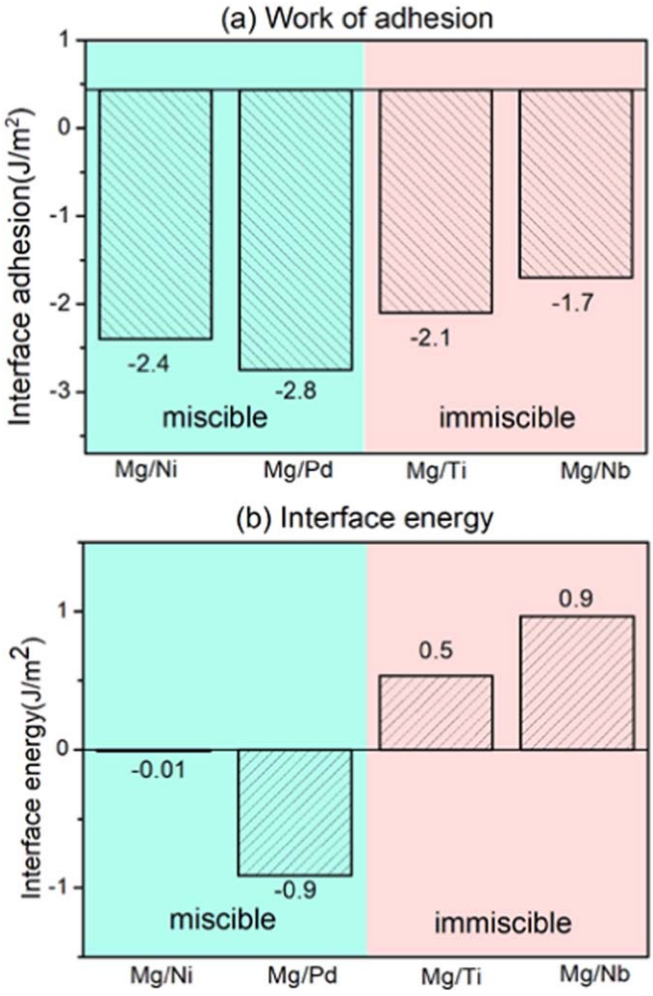

Figure 3. The work of adhesion (a) and interface energy (b) of four slab structure models with the optimized match: Mg-Ni, Mg-Pd, Mg-Ti, Mg-Nb, respectively. The light blue background corresponds to the miscible systems with Mg while the pink one represents the situation of immiscible systems.

Table 2. Details of the spacing (in Å) between layers for Mg-X interface and corresponding free surface models under corresponding strain. Here Mg 1/2 stands for the spacing between the first and second layers of Mg from the surface/interface, and correspondingly for other notations.

Model		Mg 3/4	Mg 2/3	Mg1/2	Interfacial spacing	X 1/2	X 2/3	X 3/4
Mg-Ni	Surface	2.62	2.63	2.65	/	2.01	2.03	2.04
	Interface	2.55	2.57	2.57	2.11	2.16	1.99	2.00
Mg-Pd	Surface	2.58	2.60	2.62	/	2.28	2.27	2.27
	Interface	2.62	2.66	2.62	2.08	2.31	2.29	2.29
Mg-Ti	Surface	2.57	2.56	2.56	/	2.17	2.37	2.28
	Interface	2.53	2.56	2.53	2.59	2.32	2.29	2.30
Mg-Nb	Surface	2.58	2.55	2.60	/	1.13	1.18	1.60
	Interface	2.44	2.45	2.32	2.54	0.67	0.82	1.13

spacing of Mg-Nb interface model, all of them narrowed after forming interface. It is concluded that, miscible phases tend to be close to the Mg phase while miscible phases stay away from Mg after relaxation at the interface.

3.2. Electronic Structures of Mg-X interface

Figures 4(a)–(d) show the layer-projected partial densities of states (PDOS) and charge density difference for Mg-X (X = Ni, Pd, Ti, Nb), respectively. The six layer-projected PDOS plots are corresponding to three layers of X and three layers of Mg around the interface, with the structure and charge density difference shown in the right. Here the charge density difference is defined as:

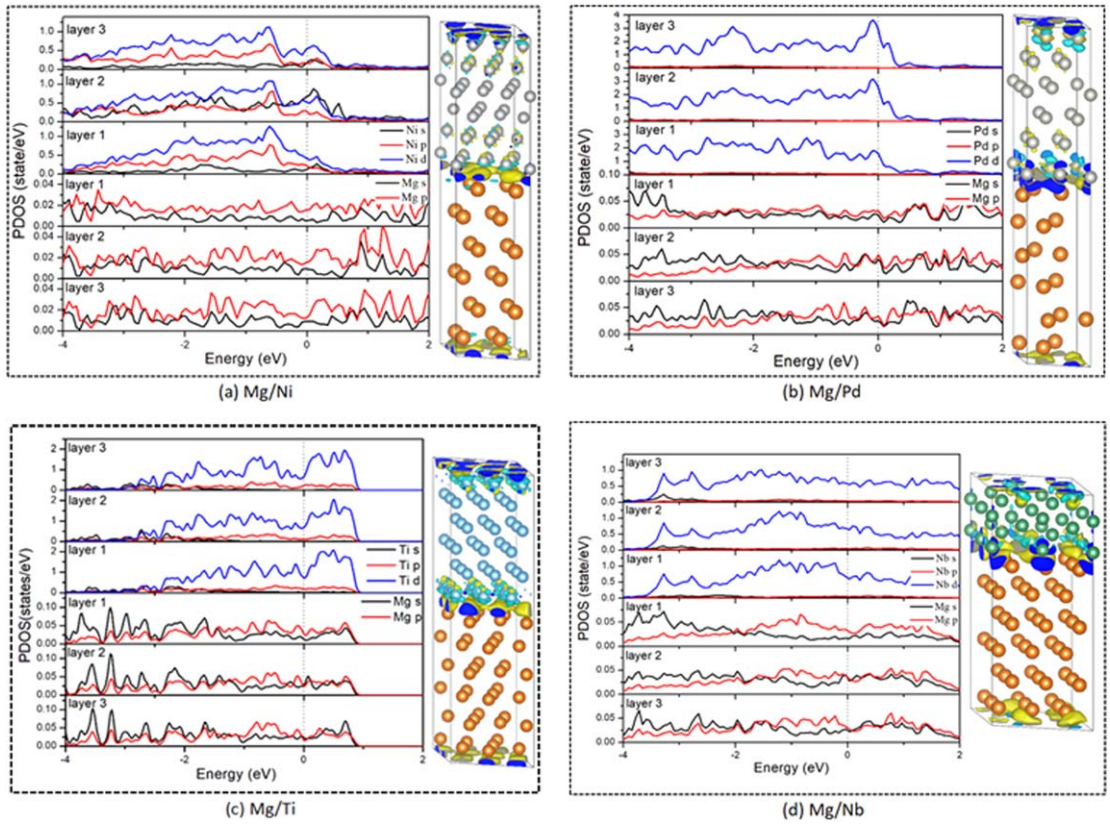

Figure 4. Layer-projected density of states and charge density difference for Mg-X interface models. The Fermi energy is set to zero. The layer numbers in PDOS correspond to the atom layer number from interface in each model. The charge density difference plots illustrate the charge redistribution when the interface forms, with yellow and green representing the depletion and accumulation of electrons, respectively.

$$\rho_{diff} = \rho^{tot}_{Mg/X} - \rho^{slab}_{Mg} - \rho^{slab}_{X}$$

Where $\rho^{tot}_{Mg/X}$ is the charge density of Mg-X interface model, while ρ^{slab}_{Mg} and ρ^{slab}_{X} are the charge densities of Mg and X slab.

For Ni system, as the layers approach the interface, it is found that the PDOS of Ni *s, p, d* are all slightly shifted towards lower energy, indicating a more stable electronic configuration at the interface. This is in good agreement with the fact that the interface of Mg-Ni system is stable with negative interface energy. For the Mg phase of Mg-Ni system, the closer to interface, the higher PDOS of *s* and *p* levels at the Fermi level, implying that hydrogen atoms will be energetically favored at the interface due to the high charge density relative to the bulk structure. It is worth noting that these trends are also available in Mg-Pd system. Through analysis of PDOS and charge density difference graphs, it is demonstrated that the closer the atoms to interface, the more stable for miscible phases as the PDOS peaks move to left nearby Fermi energy. However, the PDOS of Mg-Ti and Mg-Nb systems show the different trend around the interface. As shown in figures 4(c) and (d), there is no clear shift of PDOS with respect to the layers, so the formation of the interface does not contribute much to stability of the interface. For Mg side, it is clear that the closer the atoms to interface, the higher charge density around the Fermi level, which may be corresponding to a higher activity to hydrogen atoms.

It is clear that most of the charge re-distribution is located around the interface, contributing to form a relatively stable interface in these models. The transfer of electrons at interface accelerates the bonding between the interfacial atoms [33]. It is observed that the charge at interface mostly transfers from Mg to of the X phases, in line with their corresponding electronegativity (Pauling scale), 1.31, 1.91, 2.20, 1.54, 1.60 for Mg, Ni, Pd, Ti, Nb, respectively. Furthermore, the greater the difference in electronegativity between the two elements is, the stronger the polar bonds are. By comparing figures 4(a) and (b), it is found that the adhesion of Mg-Pd interface model is stronger, partially attributed to more electron transfers at the interface region.

3.3. Energetic and electronic properties of atomic mixing at interface

It is known that atomic mixing can occur at the interfaces, especially for miscible interfaces. Even for immiscible phases, atoms can be exchanged at the interface where the exchange can release strains at the interface for large misatch models. In order to study if the atomic mixing at interface can stabilize the interface energetically, we

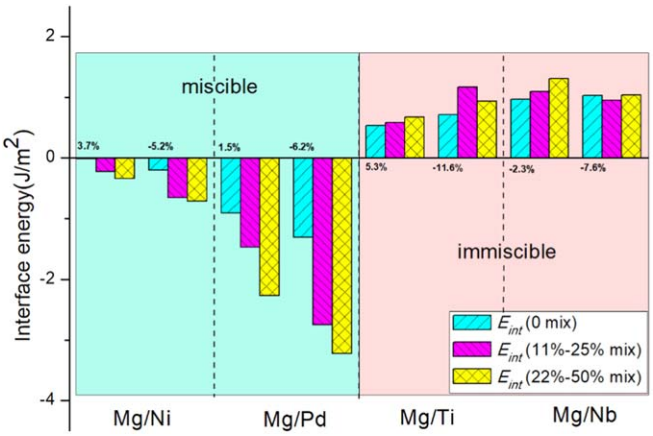

Figure 5. The interface energy corresponding to various mismatch rate and mixture rate of the interfacial atoms for the Mg-X interfaces. The light blue background corresponds to the miscible phases while the red one represents the situation of immiscible phases. The percentages in the graph represent the strain ratio of Mg in each model. Different color bars represent the interface energy of different interfacial atom mixing ratios.

have studied the interface energies of Mg-X (X = Ni, Pd, Ti, Nb), with the atom exchanges up to 50% at the first layers at the interface. We acknowledge that the atoms will be fully mixed in both phases for the miscible systems under complete theomodynamic equlibirum condition, which may not be the situation for interfaces practically. The kinetics of mixing effect, however, can be reflected by atomic exchange at first layers of the interfaces. The calculated interface energies are shown in figure 5 for various mixing percentages at the first layers. The histograms with light blue background represent the interface energies of Mg and its miscible phases (Ni and Pd), while those with pink background represent the interface energies of Mg and its immiscible phases (Ti and Nb). The percentages below or above the bars stand for the strain of corresponding mutual interfacial area relative to the ideal interfacial area of Mg with no mixing when they form interfaces. It is the mismatch of interfacial area of mutual interface models with respect to the interfacial area of ideal Mg phase. In addition to the earlier optimal interfaces, here one interface model with larger mismatch is also adopted for each Mg-X interface model to study the strain release effect from the atomic mixing. The corresponding matches of Mg-X interface with larger mismatches are $\sqrt{3}$:2, 1:1, 1:1 and 3:$\sqrt{3}$, corresponding to Mg-Ni, Mg-Pd, Mg-Ti and Mg-Nb, respectively, assuming $a = b$ in these interfaces.

The blue bars in the figures indicate the interface energies without atomic mixing. Red bars represent the interface energies of small mixing ratio (25%, 16.7%, 14.3%, 11.1% for optimal-matched and 16.7%, 25%, 25%, 11.1% for larger-mismatched interface models of Mg-Ni, Mg-Pd Mg-Ti and Mg-Nb respectively) and yellow one account for higher mixing ratio (50%, 33.3%, 28.6%, 22.2% for optimal-matched and 33.3%, 50%, 50%, 22.2% for larger-mismatched interface models of Mg-Ni, Mg-Pd Mg-Ti Mg-Nb respectively). The mixing ratio is based on the number of mixing Mg atoms with respect to the number of Mg atoms in the surface cell of the interface. For Mg-X (X = Ni, Ti and Nb) structure, one interfacial Mg atom is exchanged with interfacial X atom for small ratio mixing in the interface layer within the smallest cell in *a* and *b* direction randomly, while two Mg atoms are exchanged with two X atoms in the interface layer for a higher mixing ratio. However, for Mg-Pd structure, one interfacial Mg atoms is exchanged with interfacial Pd atom after doubling the cell in *a* or *b* direction for small ratio and two Mg atoms are exchanged with Pd for higher mixing ratio. It is clear that the Mg interfaces with mutually miscible phases are more stable than immiscible ones in any case of lattice matches. As the mismatch rate becomes larger, it is clear that the work of adhesion decrease due to the atomic mixing in the Mg interface with both miscible and immiscible phases. This is attributed to the fact that atomic mixing in interface can absorb interface strain to some extent. It is known that the radius of Mg, Ni, Pd, Ti and Nb in elemental metals are 1.59 Å, 1.24 Å, 1.40 Å, 1.44 Å and 1.43 Å, respectively. We actually have tensile strains in Mg phase for our optimal Mg-X interface models (X = Ni, Pd, Ti), therefore no strain release is expected with the atom mix at the interface as Mg has the largest atomic radius among the five elements. Consequently, the calculated interface energies become greater with the atom mixing as seen in figure 5 for the optimal interfaces. However, atom mixing may release the strain for the interfaces with larger mismatch. For the larger strain interface models, the mutual lattice constant of Mg-X (X = Ni, Pd, Ti, Nb) are 5.38 Å, 3.09 Å, 2.99 Å, 9.20 Å, respectively. The estimated strain of no atoms mixing, atoms mixing 11%–25% and atoms mixing 22%–50% interface are shown in table 3 according to the ratio of strained mutual interface area to ideal interface area of Mg phase. The plus or minus signs in the table represents the stretched and compressed state with respect to the ideal interface area of Mg.

Table 3. The estimated strain of Mg phases in the larger mismatch Mg-X (X = Ni, Pd, Ti, Nb) interface models (c.f. figure 5) with respect to the ideal Mg(0001) surface, in consideration with the atom mixing at the interface with differenct atomic radius.

Interface model	No atom mixing	Atom mixing 11%–25%	Atom mixing 22%–50%
Mg-Ni	−5.2%	−0.1%	5.5%
Mg-Pd	−6.2%	−0.03%	1.9%
Mg-Ti	−11.6%	−8.9%	−5.5%
Mg-Nb	−7.6%	−6.03%	−4.4%

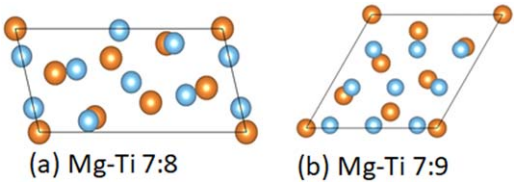

Figure 6. The 2D plot of Mg-Ti 7:8 and 7:9 interface models of the lowest energy configuration, where Mg atoms are illustrated by golden balls.

It is apparent that, for miscible phases to Mg like Ni and Pd, the interface strain drops to the lowest with 11%–25% mixing at interface, while it rises again for 22%–50% atom mixing cases. For immiscible phases to Mg like Ti and Nb, we can see that with the interfacial atom mixing ratio rises, the strains decline all the time, but the tendency of interface energy for these models is nonmonotonic, which illustrates that the miscible phase tend to separate with Mg phase.

At the interfaces with atom mixing, there would be some local structural changes around the mixing atoms after relaxation. For example, in the mixed Mg-Nb model, the Nb atoms in Mg interfacial layer move close to the Nb phase during the optimization and the mixed Nb atoms migrate 0.21 Å against the host Mg interfacial layer. Similarly, the Mg atoms in the Nb interfacial layer also move 0.55 Å far away from the layer and shift to the Mg phase. This trend can be explained by the fact that Nb is immiscible to Mg and the interaction of Mg-Nb bond is weak, so they tend to separate with each other rather than forming interface. For Mg-Ti interface model, with the atom mixing in interface, it is going to show the same trendency with Mg-Nb interface model that the mixing Ti atoms tend to move away from the host Mg interface layer and close to the Ti phase. It also occurs to the mixing Mg atoms in Ti interfacial layer and the Mg atoms tend to move far from Ti phase. Ti atom moved 0.35 Å against to the Mg host interfacial layer and Mg atom shifted 0.22 Å against to the Ti host interfacial layer. In constrast, the movement of mixing atom of Mg-Pd interface model is opposite to Mg-Nb and Mg-Ti models, as the mixing Pd atoms tend to move close to Mg phase while the mixing Mg atoms tend to move close to Pd phase during the optimization. The mixing Mg atoms in Pd interface layer move 0.30 Å close to Pd phase, while the mixing Pd atoms in Mg interface layer move 0.52 Å to Mg phase. For Mg-Ni interface model, although there is no clear movement for the mixing Mg atoms in Ni interface layer, the mixing Ni atoms in Mg interface layer still move 0.21 Å close to Mg phase during the optimization. This concludes that the miscible phases like Pd and Ni can form stable bonds with Mg, and thus the interfaces are more energetically favored with atom mixing.

As mentioned earlier, there is another possible optimal match for Mg-Ti interface, with an 8-atom cell of Ti (0001) (with $a = 2\,a_0, b = \sqrt{13}\,b_0$, included angle = 76°), which has 3.6% area mismatch to a 7-atom cell of Mg(0001) (with $a=\sqrt{3}\,a_0, b = \sqrt{53}\,b/2$, included angle = 76°). In order to check the stability of the 7:8 interface model and the corresponding mixing effect, we have further investigated this Ti-Mg interface with $a \neq b$. The 2D plot of Mg-Ti 7:8 and 7:9 (with $a = b$) interface models of the lowest energy stacking are shown in figure 6 and the calculated interface energies are listed in table 4. As noted above, although the area mismatch of 7:8 Mg-Ti interface model is smaller than the 7:9 interface model, the lattice mismatch of the 7:8 Mg-Ti interface model is much larger than 7:9 interface model. It shows that the interface energy of 7:8 model is 0.41 J m^{-2}, indeed smaller than the interface energy of 7:9 model, 0.53 J m^{-2}. This illustrates that the interface structure of 7:8 Mg-Ti model is more stable than that of 7:9 model. However, after the atomic mixing at interface, the relative stability changes. For the studied mixing ratio, the interface energy of 7:8 model is larger than the corresponding 7:9 modele, which exactly reflects the important role of interfacial atomic mixing on strain release.

The layer-projected partial densities of states (PDOS) of Mg-Ti 7:8 interface model is shown in figure 7 with corresponding atomic structure right. As similar as above PDOS plot of Mg-Ti 7:9 interface model, there is no

Table 4. The structural stability comparison of Mg-Ti interface model with matching of 7:8 and 7:9. Lattice mismatch concludes the mismatch in *a* and *b* direction.

Mg-Ti interface	7:8	7:9
Lattice mismatch	+6% and −8%	+4% and +4%
Area mismatch	−3.6%	+8.4%
E_{int}(J m^{-2})	0.41	0.53
E_{int}(14.3% mix) (J m^{-2})	0.71	0.59
E_{int}(28.6% mix) (J m^{-2})	0.87	0.67

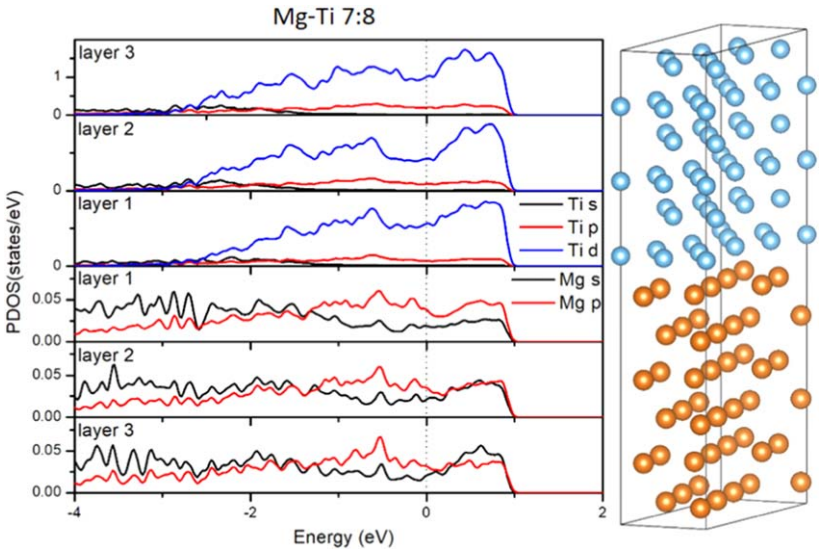

Figure 7. The layer-projected partial densities of states (PDOS) of Mg-Ti 7:8 interface model with its atomic structure at right (Mg atoms are shown in golden balls).

obvious migration of PDOS with the layer close to interface, which indicate that Mg and Ti is immiscible phase to each other again.

The electronic properties of Mg-Pd interface structure with 33.3% ratio of interfacial atomic mixing are shown in figure 8. The layer-projected partial density of states (PDOS) for Mg-Pd is calculated for the host atoms in each layer in figures 8(a) and (b), as well as the mixed atoms at corresponding interfaces. Three layers of X and three layers of Mg around the interface are included in the plot. As the layers approach the interface, the PDOS of Pd *s*, *p*, *d* are all obviously shifted towards lower energy and the trend is even more pronounced than the Mg-Pd interface model without any atom mixing at the interface (c.f. figure 8(a)), indicating a more stable electronic configuration at the interface. From figure 8(b), it is obvious that the DOS of mixed Pd atom in Mg interfacial layer mainly locates below the Fermi energy, indicating that the Pd atoms favor to mix together with Mg phase. This is in good agreement with the calculated result of structural stability that the interface of Mg-Pd system becomes more stable with atoms mixing at interface.

3.4. Kinetics of atom exchange at the interface

According to above discussion, we know that the interaction between Mg and Pd is stronger than any other studied phases with Mg. Following the investigation of Mg-Pd interface stability, we have investigated the diffusion of Mg and Pd atoms at interface to figure out the condition for the corresponding atom mixing.

The calculated diffusion coefficient D typically obeys Arrhenius behavior with respect to temperature T as [34, 35]:

$$D = D_0 \mathrm{e}^{-E_a/\mathrm{k_B}T}$$

D_0 is the pre-exponential factor of our system, for a first-order reaction. It has a unit of s^{-1}, and thus often called frequency factor. E_a is the diffusion activation energy for solutes and vacancies migrate in host phases. k_B is the Boltzmann constant and T is the temperature. From above equation, we see ln$D$ is linear with $1/T$, i.e.:

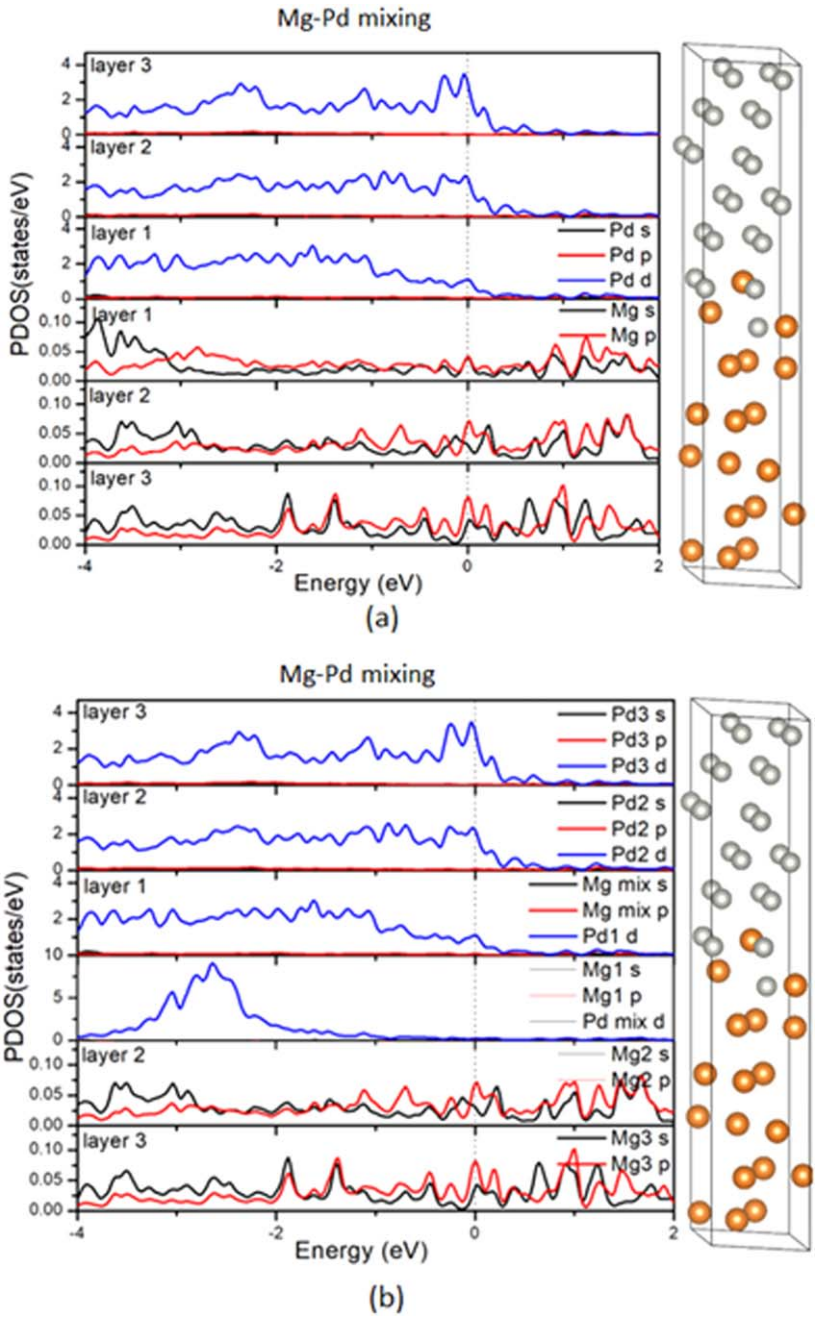

Figure 8. Layer-projected density of states for Mg-Pd mixing interface models with 33.3% mixing ratio of interfacial atoms. The Fermi energy is set to zero. The layer numbers of PDOS correspond to the atom layer number from interface in each model. Here Mg atoms are shown in golden balls.

$$\ln D = \ln D_0 - \frac{E_a}{k_B}\frac{1}{T}$$

It should be noted that E_a is related to the vacancy formation energy, solute migration energy and some influence from correlation factors. So, if the transition energy barrier is obtained, the diffusion coefficient can be estimated according the equation. The correlations for E_a and D_0 would be conductive to understanding certain features of the underlying physics of diffusion. According to the available D_0 of X in Mg [36], we find that D_0 is insensitive to nonmagnetic material X in Mg phase, so D_0 of the magnitude of 10^{-4} m^2 s^{-1} is adopted for impurity Pd in Mg phase, as well as impurity Mg in Pd phase in our study.

Before calculating the energy barrier of atoms diffusion in Mg-X interface model, we have calculated the impurity migration barriers for solute-vacancy exchange within the basal plane in Mg to ensure the accuracy of our calculation. For example, migration barriers of Ni, Pd, Nb, Ti and V in Mg are 0.98 eV, 0.96 eV, 0.94 eV, 0.67 eV, 0.88 eV, respectively, which are in good agreement with the results in literature [18], in which these migration barriers are 1.03 eV, 1.04 eV, 1.19 eV, 0.84 eV, 0.9 eV in turn. The corresponding binding energies of

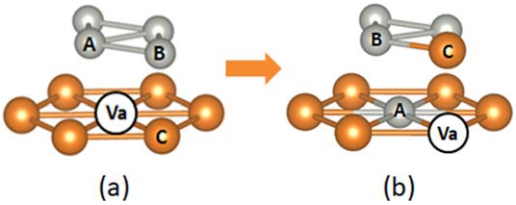

Figure 9. Initial (a) and final (b) configurations for interface atom exchange. Here, gray balls represent Pd atoms, while yellow balls represent Mg atoms.

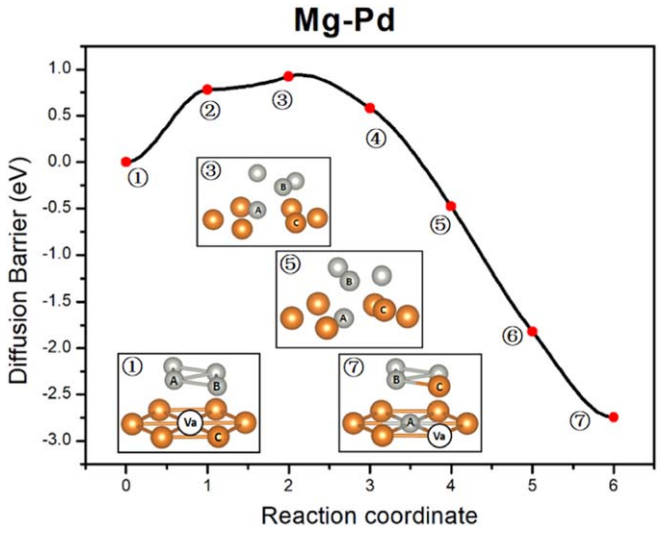

Figure 10. Diffusion route and energy barrier of atoms mixing in interface of Mg-Pd composite are shown, including the initial, final and some intermediate configurations in the transition process.

solute and vacancy were also calculated in literature [12]. Besides, the energy barriers for the collaborative diffusion, which involves 3 atoms, including a solute atom and two magnesium atoms without any vacancy are also calculated in this work. The results are 2.86 eV, 1.45 eV, 1.85 eV, 3.35 eV, 3.10 eV, 2.90 eV for Mg, Ni, Pd, Nb, Ti and V, respectively, much larger than the migration barriers with help of vacancy. So, in order for an impurity to jump in magnesium bulk, the vacancy adjacent to the impurity atom is often required [18].

The energy barrier of direct atom collaborative diffusion in Mg-Pd interface model is calculated to be 1.85 eV, which is so large that diffusion is extremely difficulty. The corresponding temperatue is estimated to be as high as 1162 K for a typical diffusion coefficient of 10^{-12} m^2 s^{-1}. In reality, vacancy is ubiquitous in bulk structures and it has played a key role in diffusion of impurity in Mg. It is found that, for Mg-Pd interface model, the interfacial vacancy would tend to stay in Mg phase rather than Pd phase after relaxation no matter the vacancy was placed at Mg or Pd side initially. The vacancy formation energies in Mg and Pd bulk are 0.84 eV and 1.20 eV, respectively, in line with the fact that vacancies are easier to form in Mg phase. When a vacancy forms adjacent to an impurity, it contributes to the diffusion process of the impurity atom [18]. Figure 9 is a schematic diagram of the initial and final state structure of the interfacial atoms diffusion process. A magnesium atom at the interface was removed to form a vacancy at the initial state. The closest Pd atom to the vacancy, atom A, represented in figure 9(a), moves to fill in the empty space, and realizing atomic mixing at the interface. Atom B fills into the original position of A consequently, and atom C migrates into the original position of B. The vacancy of final state still stays on Mg phase like initial state due to the lower vacancy formation energy in Mg than in Pd phase.

The diffusion path and the transition state of Mg-Pd interface calculated by CI-NEB are shown in figure 10. In the diffusion process, the three atoms move simultaneously. The corresponding structure of transition state appears at the third configuration. The diffusion energy barrier of atoms in the interface is about 0.94 eV. According to the above diffusion coefficient equation, the diffusion coefficient can reach 10^{-12} m^2 s^{-1} when temperature is around 590 K, which is much lower than the case without vacancy.

4. Conclusion

With a theoretical study of the structure, electronic properties of Mg-X (X = Ni, Pd, Ti, Nb) interfaces, as well as the atomic mixture effect, we conclude that:

i. As expected, the interfaces of Mg with miscible phases are more stable than those with immiscible metals. With the restriction of $a = b$, the optimal interface matches are 4:7, 3:4, 7:9, 9:4 in surface cell atom numbers (limited up to 10 in consideration of computational cost) for Mg-Ni, Mg-Pd, Mg-Ti, Mg-Nb, and the corresponding interface energies are −0.01, −0.9, 0.5, 0.9 J m^{-2}, respectively. When the lattice match is further searched without the restriction of $a = b$, Mg-Ti interface energy is lowered to 0.4 J m^{-2}, with a 7:8 cell match.

ii. Atomic mixing effect is significant for the interface stability as it changes both strain and chemical bonding at interface. For the interfaces with large mismatch, atoms mixing in interface can release interface strain significantly and stabilize the interface structures for both miscible and immiscible phases. For example, the area mismatch of Mg-Ni large interface model decreases from −5.52% to −0.1% with 16.7% atom mixing at interface. Likewise, this number of Mg-Pd large interface model drops down from −6.2% to −0.03% with 25% atom mixing at interface.

iii. Atomic exchange at the interface can occur under feasible conditions. Exemplified with Mg-Pd, the diffusion barrier is estimated to be 0.94 eV with assitance of vacancies, and the diffusion coefficiency can reach to 10^{-12} m^2 s^{-1} at temperature of 590 K.

Acknowledgments

This work is financially supported by NSFC (Grant Nos. 11574088 and 51431001), the Foundation for Innovative Research Groups of the National Natural Science Foundation of China (Grant No. 51621001), and Natural Science Foundation of Guangdong Province of China (Grant No. 2016A030312011).

ORCID iDs

Yu-Jun Zhao https://orcid.org/0000-0002-6923-1099

References

[1] Ganeshan S, Hector L G and Liu Z K 2011 *Acta Materialia* **59** 3214–28
[2] Heinz A *et al* 2000 *Materials Science And Engineering a-Structural Materials Properties Microstructure And Processing* **280** 102–7
[3] Mordike B L and Ebert T 2001 *Materials Science And Engineering a-Structural Materials Properties Microstructure And Processing* **302** 37–45
[4] Grochala W and Edwards P P 2004 *Chemical Reviews* **104** 1283–315
[5] Chen Y, Dai J, Xie R and Song Y 2016 *Surface Science* **649** 133–7
[6] Dai J H, Xie R W, Chen Y Y and Song Y 2015 *Physical Chemistry Chemical Physics* **17** 16594–600
[7] Stillesjo F, Olafsson S, Hjorvarsson B and Karlsson E 1993 *Zeitschrift fur Physikalische Chemie* **181** 353–8
[8] Baldi A, Gonzalez-Silveira M, Palmisano V, Dam B and Griessen R 2009 *Physical Review Letters* **102** 226102
[9] Trushin O, Granato E, Ying S C, Salo P and Ala-Nissila T 2002 *Physica Status Solidi B-Basic Solid State Physics* **232** 100–5
[10] Liu L M, Wang S Q and Ye H Q 2003 *Journal Of Physics-Condensed Matter* **15** 8103–14
[11] Stroppa A and Peressi M 2005 *Computational Materials Science* **33** 256–62
[12] Arya A and Carter E A 2004 *Journal Of Chemical Physics* **120** 1142–1142
[13] Wang X-G and Smith J R 2005 *Physical review letters* **95** 156102–156102
[14] Wazzan A R and Dorn J E 1965 *Journal of Applied Physics* **36** 222–8
[15] Chen K Y and Boyle K P 2012 *Physica Status Solidi B-Basic Solid State Physics* **249** 2089–95
[16] Curtin W A, Olmsted D L and Hector L G Jr 2006 *Nature Materials* **5** 875–80
[17] Yasi J A, Hector L G Jr and Trinkle D R 2010 *Acta Materialia* **58** 5704–13
[18] Zhou B-C, Shang S-L, Wang Y and Liu Z-K 2016 *Acta Materialia* **103** 573–86
[19] Picu R C and Zhang D 2004 *Acta Materialia* **52** 161–71
[20] Ganeshan S, Hector L G Jr and Liu Z K 2010 *Computational Materials Science* **50** 301–7
[21] Jiang Z T *et al* 2014 *Materials Research Innovations* **18** 137–41
[22] Wang S Q and Ye H Q 2006 *Current Opinion In Solid State & Materials Science* **10** 26–32
[23] Kresse G and Furthmuller J 1996 *Physical Review B (Condensed Matter)* **54** 11169–86
[24] Kresse G 1995 *Journal of Non-Crystalline Solids* **192–193** 222–9
[25] Blöchl P E 1994 *Physical Review* B **50** 17953–79
[26] Ernzerhof M and Scuseria G E 1999 *Journal Of Chemical Physics* **110** 5029–36
[27] Monkhorst H J and Pack J D 1976 *Physical Review B (Solid State)* **13** 5188–92
[28] Sun W and Ceder G 2013 *Surface Science* **617** 53–9
[29] Tang J-J, Yang X-B, Chen L-J and Zhao Y-J 2014 *AIP Advances* **4** 4654

[30] Liu L M, Wang S Q and Ye H Q 2003 *Surf. Interface Anal.* **35** 835–41
[31] Liu Z J, Zheng S X, Lu Z B, Pu J B and Zhang G G 2018 *Carbon* **127** 548–56
[32] Yang J H, Li B H, Wang J Z, Chen L and Li R W 2010 *J. Phys. Condens. Matter* **22** 015003
[33] Liu H X *et al* 2016 *Chin. Phys.* B **25** 211–20
[34] Agrawal P M, Rice B M and Thompson D L 2002 *Surface Science* **515** 21–35
[35] Seebauer E G and Allen C E 1995 *Progress in Surface Science* **49** 265–330
[36] Neumann G and Tuijn C 2009 *Self-Diffusion and Impurity Diffusion in Pure Metals: Handbook of Experimental Data.* (UK: Pergamon)